Inelastic transitions in slow heavy-particle atomic collisions

P. S. Krstić,[1] C. O. Reinhold,[1,2] and J. Burgdörfer[1,2,3]
[1]*Physics Division, Oak Ridge National Laboratory, Oak Ridge, Tennessee 37831-6373*
[2]*Department of Physics, University of Tennessee, Knoxville, Tennessee 37996-1200*
[3]*Institute for Theoretical Physics, Vienna University of Technology, A-1040 Vienna, Austria*
(Received 25 September 2000; published 10 April 2001)

It is a generally held belief that inelastic transition probabilities and cross sections in slow, nearly adiabatic atomic collisions decrease exponentially with the inverse of the collision velocity v [i.e., $\sigma \propto \exp(-\text{const}/v)$]. This notion is supported by the Landau-Zener approximation and the hidden crossings approximation. We revisit the adiabatic limit of ion-atom collisions and show that for very slow collisions radial transitions are dominated by the topology of the branch points of the radial velocity rather than the branch points of the energy eigensurface. This can lead to a dominant power-law dependence of inelastic cross sections, $\sigma \propto v^n$. We illustrate the interplay between different contributions to the transition probabilities in a one-dimensional collision system for which the exact probabilities can be obtained from a direct numerical solution of the time-dependent Schödinger equation.

DOI: 10.1103/PhysRevA.63.052702 PACS number(s): 34.10.+x, 34.50.Fa

I. INTRODUCTION

Ionization in slow ion-atom collisions is still a field of active research, even for systems involving one active electron. While molecular coupled-channels calculations have succeeded in describing transitions between bound states, the description of ionization requires large basis set expansions involving a quasidiscretized continuum. In the adiabatic limit, where ionization probabilities become very small, the numerical significance of results based on these methods becomes questionable. As an alternative, the hidden crossings (HC) approximation was proposed [1,2] and has been extensively used in the last decade [3–11]. A unique feature of the HC approximation is that it provides a relatively simple description of all inelastic processes (between adiabatic states of the same symmetry) on the same footing including ionization for which other theories have difficulties. This is achieved by recognizing the role of various series of transitions that promote low-lying states to the continuum.

The HC approximation was derived as an asymptotic limit for slow heavy-particle collisions and is assumed to provide the exact adiabatic limit for transitions within the states of the same symmetry. This relies on the assumption that all the information on slow collisions is contained in the adiabatic electronic energy surfaces. Assuming a straight line trajectory for the internuclear motion, the HC approximation predicts an exponential decrease of inelastic probabilities and cross sections with the inverse of the collision velocity v [i.e., $\sigma \propto \exp(-\text{const}/v)$]. Other models of nonadiabatic coupling yield similar predictions, including the celebrated Landau-Zener (LZ) approximation [12–15], and there is a wide-spread ''belief'' that the exponential behavior should be the correct adiabatic limit. However, the validity of the HC approximation and its variants has never been thoroughly tested for an exactly solvable model.

In this work we revisit the adiabatic limit for inelastic collisions. The starting point of our analysis is the adiabatic perturbation theory within which we identify the HC approximation as a limiting case when the integrand in the transition matrix element possesses only a certain class of singularities. In the HC approximation, the singularities in the electronic eigenenergy surface in the plane of complex internuclear separation R are assumed to determine inelastic transitions. This limit is also closely related to the quasiclassical (QCL) approximation for strongly forbidden transition [14]. However, when the transition matrix element possesses additional singularities, the standard result of the HC as well as QCL approximation cease to be valid and correction terms arise. In the present case of slow ion-atom collisions, additional singularities come about through zeros in the radial velocity v_R. These turning point (TP) contributions fundamentally alter the adiabatic limit. We illustrate and analyze the underlying physics of hidden crossings and the validity and the breakdown of different approximations with the help of a model for which exact transition probabilities and cross sections can be obtained from a direct numerical solution of the time-dependent Schrödinger equation. To be specific, we focus in the following discussion on slow ion-atom collisions. We emphasize, however, that the main conclusions, the deviations from an exponential behavior of inelastic transition probabilities in near-adiabatic processes due to singularities in the adiabatic transition elements have wider implications. Applications may include, for example, the response of an atom to the switching on and off of an external dc (or ac) electromagnetic field.

In Sec. II, we briefly review the adiabatic perturbation theory within the framework of molecular coupled channel approaches to slow ion-atom collisions. Limiting cases, the HC approximation, and the QCL approximation and their possible breakdown are discussed in Sec. III. An application and illustration is presented for an exactly solvable model in Sec. IV where we also illustrate the underlying physics of ''hidden'' crossings. Concluding remarks will be given in Sec. V. Atomic units are used throughout unless otherwise stated.

II. ADIABATIC PERTURBATION THEORY FOR SLOW ION-ATOM COLLISIONS

A. Molecular-orbital coupled-channel approach

Consider a typical atomic collision system involving a single active electron with coordinate $\vec{r}$ in the field of two potential wells that are separated by an internuclear distance $\vec{R}$. In a typical scattering experiment, the electron is initially prepared in a bound state of the two-center quasimolecular field of the potential wells while the internuclear motion has a well-defined collision velocity $v=P_i/\mu$, P_i and μ being the internuclear momentum and the reduced internuclear mass, respectively. In the following, we adopt a time-dependent approach in which the internuclear motion follows a single classical trajectory, $\vec{R}=\vec{R}(t)$. In particular, we assume that the collision energy is large enough in comparison to the characteristic transition energies, such that we can employ a straight-line trajectory $\vec{R}=\vec{b}+\vec{v}t$, where b is the impact parameter. This choice is motivated by the fact that within a time-dependent approach the steps that lead to the HC and QCL approximations as well as to their breakdown due to turning point effects become transparent. The time-dependent approach furthermore lends itself to a straightforward generalization to other time-dependent problems such as perturbations by external fields. However, we will present in Sec. IV also calculations including the fully quantum description of the nuclear motion that confirms the conclusions obtained using a classical trajectory $R=R(t)$ and rules out the presence of artifacts due to the impact-parameter approximation.

Within a time-dependent approach, the evolution of the electronic wave function $|\Psi(t)\rangle$ is governed by the time-dependent Schrödinger equation

$$i\frac{d|\Psi(t)\rangle}{dt}=H_{\rm el}(\vec{R})|\Psi(t)\rangle \tag{1}$$

with the electronic Hamiltonian

$$H_{\rm el}[\vec{R}(t)]=-\frac{\nabla_{\vec{r}}^2}{2}+V_T[|\vec{r}-\vec{R}_T(t)|]+V_P[|\vec{r}-\vec{R}_P(t)|], \tag{2}$$

where V_T and V_P represent the interaction with the moving target and projectile potential wells centered at R_T and R_P (i.e., $\vec{R}=\vec{R}_P-\vec{R}_T$), and we use a coordinate system centered at the center of mass of the collision system. Here we are concerned with slow ion-atom collisions in which the time variation of $R(t)$ (i.e., the radial velocity $v_R=dR/dt$), is much smaller than the atomic and molecular time scales. Thus, the time evolution of the state of the electron $|\Psi(t)\rangle$ is best described in terms of the adiabatic eigenstates $|\phi_n(\vec{R})\rangle$ of the Hamiltonian,

$$H_{\rm el}(\vec{R})|\phi_n(\vec{R})\rangle=E_n(R)|\phi_n(\vec{R})\rangle, \tag{3}$$

where $\vec{R}(t)$ is treated as a an external parameter. We will frequently interchange R with t as the control parameter, e.g., $E_n(t)=E_n[R(t)]$.

The time evolution of the collision system can be obtained using an expansion of the electronic wave function, $|\Psi(t)\rangle$, in the adiabatic states

$$\Psi(\vec{r},t)=\sum_n A_n(t)\chi_n(\vec{r},t), \tag{4}$$

where

$$\chi_n(\vec{r},t)=\phi_n[\vec{r},\vec{R}(t)]\exp\left(-i\int_0^t dt'\,E_n[R(t')]\right) \tag{5}$$

and we have purposely ignored translation factors (for simplicity) since they should become negligible in the adiabatic limit (a treatment with translation factors can be found elsewhere [2]). Inserting Eq. (4) into the time-dependent Schrödinger equation, one obtains the standard molecular-orbital coupled-channels (MOCC) approach given by the set of coupled equations [16]

$$i\frac{dA_n}{dt}=\sum_k A_k(t)\langle\chi_n(t)|H_{\rm el}-i\frac{d}{dt}|\chi_k(t)\rangle. \tag{6}$$

The transition amplitude or S matrix element for the transition $i\to f$ is given by

$$S_{f,i}=\lim_{T\to\infty}A_f(T). \tag{7}$$

where Eq. (6) is solved subject to the initial condition

$$\lim_{T\to-\infty}A_n(y)=\delta_{ni}. \tag{8}$$

Numerical MOCC approaches attempt to solve Eq. (6) for a large but finite number of channels k. Apart from truncation errors (finite k) Eq. (6) is an exact representation of the original Schrödinger equation.

The key ingredient in Eq. (6) that determines the time evolution is given by the nonadiabatic coupling between the adiabatic states, $\langle\chi_n(t)|H_{\rm el}-id/dt|\chi_k(t)\rangle$. In general, the dynamics of the collision system involves both radial and rotational couplings. For simplicity, we focus in the following only on adiabatic radial couplings

$$U_{f,i}(R)=\langle\phi_f(R)|\frac{d}{dR}|\phi_i(R)\rangle. \tag{9}$$

Extensions of the present analysis to rotational coupling is straightforward. We set

$$\langle\chi_n(t)|H_{\rm el}-i\frac{d}{dt}|\chi_k(t)\rangle=-i\frac{dR}{dt}U_{n,k}(t)\times\exp\left[i\int_0^t dt'\,\Delta E_{n,k}[R(t')]\right], \tag{10}$$

where, $\Delta E_{n,k}[R(t)]=E_n[R(t)]-E_k[R(t)]$. Nonadiabatic transitions are introduced by allowing the perturbation parameter $R(t)$ and, hence, the Hamiltonian to become slowly time-dependent. The key parameter that controls the adiabaticity of the process is the speed of the parametric deformation, the radial velocity $v_R=|dR(t)/dt|$.

B. Perturbation theory

Equation (6) can be approximately solved within the framework of adiabatic perturbation theory. The fundamental assumption is that v_R is ''small,'' $v_R \ll 1$. Consequently, the coupling between different molecular orbitals [Eq. (10)] is ''weak.'' To leading order, the electronic wave packet can follow the adiabatic electronic eigenenergy surface $E_i(R)$ and is only weakly perturbed when $E_i(R)$ approaches another eigenenergy surface $E_f(R)$ near an avoided crossing (AC). As we will discuss below, the concept of avoided crossings can be generalized to HC. Equation (6) can therefore be solved iteratively by setting $A_i=1$ on the right-hand side giving the first-order perturbation theory (up to an overall phase) [17–19]

$$S_{f,i}=-\int_{-\infty}^{\infty} dt \frac{vt}{\sqrt{(vt)^2+b^2}} U_{f,i}[R(t)] \times \exp\left[-i\int_D^t dt' \Delta E_{f,i}[R(t')]\right], \tag{11}$$

where we have used the explicit time dependence $R(t)=\sqrt{v^2t^2+b^2}$ in the radial velocity $v_R=vt/\sqrt{b^2+(vt)^2}$. Since $R(t)$ is not a monotonic function of t, $v_R(t)$ reverses its sign at the TP at $t=0$ and $R(0)$. In addition, $R(t)$ is an even function of t, and Eq. (11) becomes

$$S_{f,i}=-2i\,\mathrm{Im}\left\{\int_{-\infty}^{\infty} dt \frac{vt}{\sqrt{(vt)^2+b^2}} U_{f,i}[R(t)] \times \exp\left[-i\int_0^t dt' \Delta E_{f,i}[R(t')]\right]\right\}. \tag{12}$$

In terms of the parameter R, the S matrix element reads

$$S_{f,i}=-2i\,\mathrm{Im}\left\{\int_{R(0)}^{R(\infty)} dR\, U_{f,i}(R) \times \exp\left[i\int_{R(0)}^{R} \frac{\Delta E_{f,i}(R')}{|v_{R'}|} dR'\right]\right\}. \tag{13}$$

Contributions to $S_{f,i}$ come from regions where $U_{f,i}(R)$ is ''large'' or $\Delta E_{f,i}(R)$ is ''small.'' In view of the analytic structure of the electronic eigenenergy surface those two properties are, in fact, intimately connected to each other. This observation serves as the starting point for the development of the HC approximation. Generically, perturbation theory and semiclassical approximations are complementary to each other. Semiclassical or quasiclassical approximations require large action, $\int E_{i,f}(t)dt/\hbar \gg 1$, in natural units. In turn, perturbation theory requires, in general, small changes in the phase of evolution of the wave packet, $\int E_{i,f}(t)dt/\hbar \ll 1$. Adiabatic perturbation theory is special in the sense that it requires weak coupling rather than small actions. Therefore, quasiclassical approximations and perturbation theory may be closely related, in special cases even coincide, for near-adiabatic processes. Equation (12) indicates, furthermore, that in addition to singularities of the energy surfaces also additional singularities in the integrand, specifically in v_R, may give additional contributions to $S_{f,i}$. This observation will lead us to the development of corrections to the HC approximation in terms of TP contributions.

For the following discussion it is useful to delimit the regime of ''slow'' velocities more precisely: we consider velocities small compared to the so-called ''Massey maximum'' at which typically inelastic transition probabilities peak,

$$v_R \lesssim v \ll v_{\max} \approx |\Delta E_{i,f}(R\to\infty)|\,a, \tag{14}$$

where $\Delta E_{f,i}(R\to\infty)$ is the asymptotic separation of the energy levels and $R=a$ is the ''adiabatic radius'' where atomic systems effectively begin to couple ($a\approx 1$ a.u.). On the other hand, our adiabatic limit $v\to 0$ is understood to exclude the threshold region for the breakup of the composite molecular system, i.e.,

$$v > \sqrt{2[\Delta E_{i,f}(R\to\infty)]/\mu}, \tag{15}$$

where the reduced mass of the quasimolecular system is $\mu \gtrsim 10^3$.

III. HIDDEN CROSSING AND QUASICLASSICAL APPROXIMATIONS

In this section we discuss the approximate evaluation of Eqs. (12) and (13) within the framework of the so-called HC approximation and show its close connection to the QCL approximation. It should be emphasized that both approximations go back to the pioneering work of Landau [12] who realized early on that energy surfaces in the complex parameter plane [20] determine, to a considerable degree, the S matrix in the near-adiabatic limit.

A. Hidden crossing approximation

An implicit and, as will be shown, sometimes erroneous assumption of the HC approximation is that the R region near the inner turning point, $R(0)$, in Eq. (13) does not yield a significant contribution to the transition. Specifically, we assume, for the moment, the coupling does vanish identically at the turning point, $U(R)=0$ for $R\leq R(0)$. We then can extend the integral over the entire real R axis to give

$$S_{f,i}^{\mathrm{HC}}=-2i\,\mathrm{Im}\left\{\int_{-\infty}^{\infty} dR\, U_{f,i}(R)\exp\left[i\int_0^R \frac{\Delta E_{f,i}(R')dR'}{v_{R'}}\right]\right\}. \tag{16}$$

This integral can be evaluated by contour integration. Within this approximation, the analytic structure of the en-

ergy surface and of the coupling matrix element in the complex R determines the S matrix.

Singularities in the energy surface and in the adiabatic coupling-matrix elements are, in fact, intimately connected. We illustrate this connection with the help of a two-state model that captures the essence of the pairwise interaction of two adiabatic energy curves $E_i(R)$ and $E_f(R)$ undergoing an avoided crossing with each other. At this point we do not make a distinction between clearly visible ACs or HCs as they possess similar properties in the complex plane. Physical differences will be discussed later. A critical distance at which the energy separation between the two adiabatic energy curves is smallest will be denoted by R_{AC} (or R_{HC}). We introduce the corresponding two diabatic states $|\psi_1\rangle$ and $|\psi_2\rangle$ that do not diagonalize H_{el} but, instead, are defined through a vanishing of the coupling by the operator d/dR. By construction, diabatic states are smooth (singularity free) functions of R near R_{AC}. Note that such a definition of diabatic states is only locally meaningful [16,21].

The adiabatic energies can be obtained by diagonalization of the Hamiltonian matrix (with matrix elements $H_{jk}=\langle\psi_j|H_{\mathrm{el}}|\psi_k\rangle$) in the diabatic basis as

$$E_{f,i}(R)=\overline{E}(R)\pm\Delta E_{f,i}(R), \tag{17}$$

$$\overline{E}(R)=\frac{H_{ii}(R)+H_{ff}(R)}{2}, \tag{18}$$

$$\Delta E_{f,i}(R)=\tfrac{1}{2}\sqrt{[H_{ii}(R)-H_{ff}(R)]^2+4|H_{if}(R)|^2}. \tag{19}$$

For real values of R, the adiabatic level splitting $\Delta E_{f,i}(R)$ has a local minimum (avoided crossing) at R_{AC} or $R_{\mathrm{HC}}=\mathrm{Re}\{R_c\}$ where $H_{ii}(R)=H_{ff}(R)$. The level splitting becomes zero for complex values $R=R_c$, R_c^* such that $H_{ii}(R)-H_{ff}(R)=\pm i2H_{if}(R)$. Obviously, expansion of the argument of the square root in Eq. (19) to first order around $R=R_c$, R_c^* yields

$$\Delta E_{f,i}(R\approx R_c)=C\sqrt{R-R_c},\quad \Delta E_{f,i}(R\approx R_c^*)=C^*\sqrt{R-R_c^*} \tag{20}$$

where C is a constant that depends on the matrix elements of H_{el} and their first derivatives with respect to R. Equation (20) shows that the adiabatic energies E_i and E_f are two Riemann sheets of the same multivalued eigenenergy surface and that the intersection points of the adiabatic energies have the form of square-root branch points. Thus, for the incoming phase of the collision, starting on the branch E_i at $E_i(R_1=\mathrm{Re}\{R_c\}+\epsilon)$ (where ϵ is a small positive number) and moving on the complex-R plane such that R_c is encircled, we would end up on E_f at $E_f(R_2=\mathrm{Re}\{R_c\}-\epsilon)$ upon return to the real axis (Fig. 1).

This two-state analysis can be generalized to many states with the result that the analytic continuations of $\phi_n(\vec{r},\vec{R})$ and $E_n(R)$ onto the complex R plane for states of the same symmetry are various branches of single, multivalued and multiply connected eigenfunctions and eigenenergies. The branch points are the complex points of transition and are called either avoided crossings when the branch point lies close to the real axis (i.e., $\mathrm{Im}\{R_c\}$ small) or hidden crossings when the distance to the real axis is large. This terminology originates from the fact that in the latter case an avoided crossing is hardly recognizable in the cut through the energy surface along the real axis. The topology of the adiabatic eigenenergy surface has immediate implications for the nonadiabatic couplings determining electronic transitions [Eqs. (6)–(11)]. In order to show this consequence, it is convenient to introduce an unitary transformation between the diabatic, $\{\psi_i(R)\}$, and adiabatic basis, $\{\phi_i(R)\}$, defined as [22]

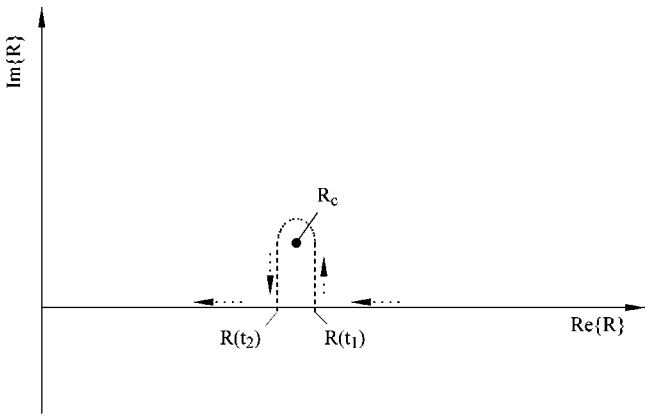

FIG. 1. Typical evolution path in $R(t)$ domain in the hidden crossings method, for a two-state collision system.

$$\phi_i(R)=\cos\theta\psi_i(R)+\sin\theta\psi_f(R),$$

$$\phi_f(R)=\cos\theta\psi_f(R)-\sin\theta\psi_i(R), \tag{21}$$

where

$$\sin\theta=\left[\frac{1}{2}\left(1-\frac{1}{(1+\eta^2)^{1/2}}\right)\right]^{1/2}$$

$$\cos\theta=\left[\frac{1}{2}\left(1+\frac{1}{(1+\eta^2)^{1/2}}\right)\right]^{1/2} \tag{22}$$

and

$$\eta=\eta(R)=\frac{H_{ff}(R)-H_{ii}(R)}{2H_{if}(R)}. \tag{23}$$

For definiteness let us assume, $H_{ff}(R\to\infty)>H_{ii}(R\to\infty)$, and H_{if} to be nonzero near R_{AC} but $H_{if}(R\to\infty)\to 0$, for real R. The function $\eta(R)$ is assumed to be monotonic but otherwise arbitrary. Well known, analytically solvable models such as the LZ model result from particular choices for $\eta(R)$.

The radial coupling between the two adiabatic states [Eq. (19)] takes now the form

$$U_{f,i}(R)=\frac{1}{4}\frac{d\eta}{dR}\frac{1}{1+\eta^2}, \tag{24}$$

which possesses simple poles at $\eta=\pm i$. Expanding η to first order near $R\approx R_c$ yields

$$\eta \approx C(R-R_c)/2H_{12}(R_c)+i, \tag{25}$$

and inserting this result in Eq. (24),

$$U_{f,i}(R\approx R_c)\approx -\frac{i}{4}\frac{1}{R-R_c}, \quad U_{f,i}(R\approx R_c^*)\approx \frac{i}{4}\frac{1}{R-R_c^*}, \tag{26}$$

shows that nonadiabatic matrix elements have poles exactly at the branch points of the eigenenergy surfaces [2]. Along the real R axis, $U_{f,i}$ exhibits peaks in the vicinity of $R_{\rm AC}$ or $R_{\rm HC}=\mathrm{Re}\{R_c\}$ and determines the region of R values here nonadiabatic transitions take place.

These observations deduced from a two-state analysis can be generalized for any electronic Hamiltonian $H_{\rm el}(R)$ that is a memomorphic function of complex R, i.e., possesses only isolated branch points in the complex plane [3,6,8–10]. Accordingly, its eigenfunctions $\phi_n(\vec{r},\vec{R})$ and eigenenergies $E_n(R)$ have isolated branch points in the complex plane as well, which appear in complex-conjugated pairs, as follows from the Schwarz's reflection principle: If $\phi_n(\vec{r},\vec{R})$ is real for real R, then $\phi_n(\vec{r},\vec{R}^*)=\phi_n^*(\vec{r},\vec{R})$ and $E_n(R^*)=E_n^*(R)$. Both $\phi_n(\vec{r},\vec{R})$ and $E_n(R)$ are analytic continuations of their respective functions for real R. All adiabatic energy levels are part of a unique, multivalued adiabatic energy surface $E(R)$ in the plane of complex R. Different energy levels correspond to the intersection of different Riemann sheets of this energy surface with the $(E,\mathrm{Re}\{R\})$ plane [3,6,8–10] that are connected in the complex-R plane in a pairwise fashion. $H_{\rm el}$ is complex symmetric if it is symmetric and Hermitian for real R [23]. The eigenfunctions $\phi_n(\vec{r},\vec{R})$ form a biorthonormal basis [19,24], i.e., $\int d^3r\ \phi_i^*(\vec{r},\vec{R}^*)\phi_j(\vec{r},\vec{R})=\delta_{ij}$. These functions can be written as $\phi_n(\vec{r},\vec{R})=C_n(R)\chi_n(\vec{r},R)$, where χ_n are biorthogonal but are not normalized. At the point of intersection $R=R_c$ of $E_i(R)$ and $E_j(R)$, $i\neq j$, the two eigenfunctions $\phi_i(\vec{r},\vec{R}_c)$ and $\phi_j(\vec{r},\vec{R}_c)$ coincide, and thus $\int d^3r\ \phi_i^*(\vec{r},\vec{R}_c^*)\phi_j(\vec{r},\vec{R}_c)=1$. On the other hand, $\int d^3r\ \chi_i^*(\vec{r},\vec{R}_c^*)\chi_j(\vec{r},\vec{R}_c)=0$ for any $i\neq j$. In order to satisfy both conditions, the normalization constant $C_n(R)$ has to be algebraically singular at R_c [2]. These properties can be directly verified for the two-state system [Eqs. (21) and (22)]. As a consequence of the singularity in $C_n(R)$, matrix elements of operators that are functions of the differential operator, $F(d/dR)$, $\int d^3r\ \phi_i^*(\vec{r},\vec{R}^*)F\phi_j(\vec{r},\vec{R})$ are also singular at $R=R_c$ [2,3]. The most important example is the radial coupling matrix element $U_{i,f}$ that possesses poles at R_c [see Eq. (26)].

With the knowledge of the poles in the coupling matrix elements and the branch points in the energy surface, Eq. (16) can be evaluated by contour integration. Taking into account only one branch point connecting two Riemann surfaces of the two-state system, we find for the contribution from R_c (up to a phase factor)

$$S_{f,i}^{\rm HC}=(P_{f,i}^{\rm HC})^{1/2}\exp(i\xi_{f,i}), \tag{27}$$

where

$$P_{f,i}^{\rm HC}=\exp(-2|\mathrm{Im}\{\omega_c\}|), \tag{28}$$

$$\omega_c=-\int_C dR E(R)/v_R, \tag{29}$$

$$\xi_{f,i}=\mathrm{Re}\{\omega_c\}, \tag{30}$$

In Eq. (29) the contour encircles the branch point (Fig. 1) involving the Riemann sheets of E_i and E_f. Equation (28) displays the exponential decay of probability predicted by the HC approximation in the adiabatic limit.

B. Quasiclassical approximation

As pointed out by Landau [14], the adiabatic limit of the inelastic transition probability can be alternatively derived within the framework of a QCL approximation. Semiclassical or quasiclassical approximations are valid when the potential is smooth on a scale of the de Broglie wavelength Λ. Remarkably, this statement remains valid when Λ is purely imaginary, i.e., $|\Lambda|$ is sufficiently small. Dynamical tunneling processes become quasiclassical when the action along the complex trajectories is large. In the present case this implies

$$\left|\mathrm{Im}\left(\int [E(R)]dR/v_R\right)\right| \gg 1. \tag{31}$$

The remarkable observation connected with Eq. (31) is that classically strongly forbidden (such as wide-barrier tunneling) processes are accessible to a quasiclassical approximation.

The transition between two adiabatic potential curves near an AC or HC is formally equivalent to the one-dimensional overbarrier reflection problem, transcribed to the time domain. The transmitted wave ψ_T corresponds to the propagation on the adiabatic potential surface E_i,

$$\psi_i^{\rm QCL}(t_2)\propto \exp\left(-i\int_{-\infty}^{t_2} dt' E_i(t')\right). \tag{32}$$

Note that, within the QCL approximation preexponential factors are assumed to be slowly varying compared to the rapidly varying exponent [Eq. (31)]. The turning point (or transition point) for ''overbarrier'' reflection lies at complex t_C (or R_C). Analogously, the quasiclassical reflected wave is given by

$$\psi_R^{\rm QCL}(t)\propto \exp\left[-i\left(\int_{-\infty}^{t_1} dt\, E_i(t)+\int_{t_1}^{t_c} E_i dt+\int_{t_c}^{t_2} E_f dt\right)\right]. \tag{33}$$

Accordingly, the reflection amplitude is given by the ratio of the reflected to transmitted wave,

$$r^{\mathrm{QCL}} = \psi_R^{\mathrm{QCL}}(t_2)/\psi_T^{\mathrm{QCL}}(t_2) = \frac{\exp[-i\int_{-\infty}^{t_c} E_i(t')dt - \int_{t_c}^{t_2} E_f(t')dt']}{\exp[-i\int_{-\infty}^{t_2} dt' E_i(t')]} = \exp\left[-t\int_C E[R(t')]dt'\right]. \tag{34}$$

The contour along which the integral over the multivalued energy surface is evaluated corresponds to the one shown in Fig. 1. The reflection amplitude [Eq. (34)] is therefore completely equivalent to $S_{f,i}^{\mathrm{HC}}$ [Eq. (27)]. The quasiclassical approximation subject to the condition that preexponential factors are set to 1 coincides with the HC approximation.

C. Two-state Landau-Zener approximation

The celebrated LZ approximation [12,13,15] is a special case of a two-state system with a single avoided crossing. It results from the following assumptions for the diabatic matrix elements [see Eqs. (17)–(19)]:

$$H_{22}(R) - H_{11}R = G(R - R_{\mathrm{AC}}) = \mathrm{const}\times(R - R_{\mathrm{AC}}), \tag{35}$$

$$v_R = \mathrm{const}, \tag{36}$$

$$H_{12}(R) = \mathrm{const}. \tag{37}$$

For this set of parameters, the two-state MOCC equations [Eq. (6)] in its diabatic representation can be solved exactly and analytically. Expressed in terms of either the diabatic LZ parameters [Eqs. (35)–(37)] or the parameters of the adiabatic potential surfaces, the probability for a transition can be written as

$$P_{f,i}^{\mathrm{LZ}} = \exp(-\pi\mu_c) = \exp\left(-\frac{2\pi|H_{12}|^2}{G v_R}\right) = \exp\left(-\frac{\pi|\Delta E_{f,i}(R_{\mathrm{AC}})|\mathrm{Im}\{R_c\}}{2v_R}\right), \tag{38}$$

where $\mu_c = |\Delta E_{f,i}(R_{\mathrm{AC}})|\mathrm{Im}(R_c)/(2v_R)$ is the Massey parameter of the transition that determines the ''strength'' of a nonadiabatic transition. In Eq. (38) we exploited the correspondence between the parameters in the adiabatic and diabatic representations, $G = \Delta E_{f,i}(R_{\mathrm{AC}})/\mathrm{Im}\{R_c\}$ and $2H_{12} = \Delta E_{f,i}(R_{\mathrm{AC}})$. The point of intersection of the adiabatic terms in the complex-R plane is given by $R_c = R_{\mathrm{AC}} \pm i2H_{12}(R_{\mathrm{AC}})/G$. The parameter $\eta(R)$ in Eq. (23) takes the form $\eta = (R - R_{\mathrm{AC}})/\mathrm{Im}\{R_c\}$, which yields

$$E_f(R) - E_i(R) = \frac{\Delta E_{f,i}(\mathrm{Re}\{R_c\})}{\mathrm{Im}\{R_c\}}\sqrt{(R - R_c)(R - R_c^*)}, \tag{39}$$

$$U_{fi}^{\mathrm{LZ}}(R) = \frac{1}{2}\frac{\mathrm{Im}\{R_c\}}{(R - \mathrm{Re}\{R_c\})^2 + (\mathrm{Im}\{R_c\})^2}. \tag{40}$$

This Lorentzian shape just follows from the sum of the matrix elements in Eq. (26), obtained in the vicinity of R_c and R_c^*.

It should be noted that the assumptions [Eqs. (35)–(37)] were previously used as the leading terms of the expansions in R in the immediate vicinity of R_c [Eqs. (21)–(25)]. Within the LZ model, the validity of Eqs. (35)–(37) is assumed globally for all R. It is this property that allows for an exact analytical solution. The global extension to all R should not obscure the fact that the LZ approximation is still only a locally applicable model since the underlying assumptions, the asymptotic divergence of adjacent energy levels of the same symmetry, i.e., $|H_{11} - H_{22}| \to \infty$ as $R \to \infty$ as well as $H_{12} = \mathrm{const}$ are unphysical. The significance of this model is that the exponentially suppressed transition probability can be determined exactly in complete agreement with Eqs. (28) and (34).

The limitations concerning the vicinity of the turning points and R_{AC} are serious. These were first taken into account by Bykhovskii, Nikitin, and Ovchinnikova [25], who assumed the constant acceleration approximation for the velocity, keeping the linearity of the diabatic terms as well as constant coupling, like in the LZ model. Further improvement was obtained by Delos and Thorson [26], who accounted for some effects of variation of H_{12} and curvature of the diabatic terms, as well as for the nuclear acceleration [27]. The common conclusion was that since the LZ probability increases steeply with velocity, the effect of acceleration is to increase the transition probability at low velocities, in the vicinity of the turning point.

One important insight that can be gained from the LZ model is that of the degree of localization of the nonadiabatic transitions. Transitions effectively occur only in a very narrow region $|\Delta R|$ outside of which no net transfer of probability between terms takes place. The Lorentzian form of U_{fi}^{LZ} in Eq. (40) provides an upper bound of the localization range of the transitions $|\Delta R| \lesssim \mathrm{Im}\{R_c\} = 2H_{12}/G$. For $|R - R_{\mathrm{AC}}| > |\Delta R|$ the adiabatic states become effectively decoupled. However, this estimate does not take into account the rapidly changing phases involved in the transition probabilities per unit time in the adiabatic limit $v \to 0$. For a two-state model the relevant phase in the diabatic representation is given by $\int dR[H_{11}(R) - H_{22}(R)]/v_R$. This rapidly oscillating phase implies that in the limit $v_R \to 0$ the transition probability tends to zero. Using Eqs. (35)–(37) the phase becomes $G(R - R_{\mathrm{AC}})^2/(2v_R)$ and the localization length of the transition can be estimated from the distance from R_{AC} where the phase is of the order of unity [19],

$$\Delta R \sim \left[\frac{v_R}{G}\right]^{1/2} = \left[\frac{\mathrm{Im}\{R_c\}v_R(R_{\mathrm{AC}})}{\Delta E_{f,i}(R_{\mathrm{AC}})}\right]^{1/2}. \tag{41}$$

The same result can be obtained from the exact Landau-Zener solution. Equation (41) implies that transitions are ''perfectly'' localized ($\Delta R \to 0$) in the adiabatic limit, $v_R \to 0$, provided, however, that v_R remains constant within the transition region. The assumption $v_R = \mathrm{const}$ is also essential and can become a serious limitation if R_{LZ} is close to

region of the classical turning point. An analysis of such limitations can be found in [26,25].

The strong localization of a transition between pairs of levels is the starting point of the generalization of the HC approximation for multilevel systems.

D. Multilevel hidden crossing approximation

The observation that the pairwise interaction between levels is fairly localized, opens up the possibility to describe the evolution for a multilevel system as a sequence of localized transitions followed by an unperturbed evolution on a given potential curve until the next crossing occurs. For each localized transition between levels i and j we can describe the evolution operator U_C as a direct sum of a unit operator for all other levels and a 2×2 matrix in the subspace (i,j) [7,19],

$$\mathcal{U}_C(R_C)=1\oplus\mathcal{U}_C^{(i,j)}(R_C) \tag{42}$$

with

$$\mathcal{U}_C^{(ij)}=\begin{bmatrix} \sqrt{1-P_{i,j}^{\mathrm{HC}}} & \sqrt{P^{\mathrm{HC}}}\exp(i\xi_{i,j}) \\ \sqrt{P_{ij}}\exp(\xi_{i,j}) & \sqrt{1-P_{i,j}^{\mathrm{HC}}} \end{bmatrix}. \tag{43}$$

In Eq. (43) we have used the transition amplitude [Eq. (27)] as off-diagonal element and have unitarized the matrix by correcting the diagonal elements for loss of probability. Between two sequential hidden crossing regions at t_k and t_{k+1}, the adiabatic evolution is given by a diagonal matrix U_d in the adiabatic basis

$$\mathcal{U}_d(t_{k+1},t_k)=\mathrm{diag}\left\{\left[\exp\left(-i\int_{t_k}^{t_{k+1}}E_j(t)dt\right)\right]_{j=1,\ldots}\right\}. \tag{44}$$

For convenience we have switched in Eq. (44) from R to the time t as the parameter for the evolution.

Consequently, for a collisional system involving many states, the evolution operator can be written as a product of localized transition matrices [7,19] in the infinitesimal vicinity of the hidden crossings and diagonal matrices representing the adiabatic evolution of the system between transition points, i.e.,

$$\mathcal{U}(-\infty,\infty)=\prod_k \mathcal{U}_C(t_k)\mathcal{U}_d(t_{k+1},t_k). \tag{45}$$

If a large number of branch points and adiabatic energy curves are involved, the direct determination of Eq. (45) involves a comparable level of complexity as the direct numerical solution of the MOCC equation [Eq. (6)]. As an alternative to Eq. (45) a multilevel HC approximation has therefore been devised by which the MOCC equations are numerically solved, however, with the exact adiabatic coupling matrix elements $U_{i,j}(R)$ replaced by localized Lorentzian (or hidden crossing) couplings $U_{i,j}^{\mathrm{LZ}}$ [Eq. (40)] resulting from the poles [Eq. (26)] valid only in the vicinity of the hidden or avoided crossing. We refer to this method as the close-coupling hidden crossing (CCHC) method. To a good degree of approximation, the CCHC method should be equivalent to Eq. (45). The couplings $U_{i,j}^{\mathrm{LZ}}$ tend sufficiently fast to zero at $R\to\infty$, and do not depend on the electron origin (a common problem in some MOCC calculations [28]). Note that the asymptotic behavior of the coupling far from R_{AC}, $U_{i,j}^{\mathrm{LZ}}\propto 1/R^2$, is not necessarily correct. However, as long as the transitions are strongly localized about the hidden crossings, the actual behavior of the exact nonadiabatic coupling far from the crossing is irrelevant. The CCHC approach should become increasingly inaccurate if the transitions are not localized or well separated from each other, depending on the parameters of the system as well as on the collision velocity.

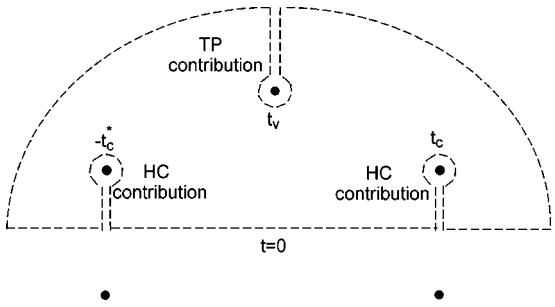

FIG. 2. Contour of integration in the complex time domain to evaluate the S matrix.

E. TP effects

We return now to the original expression of the two-state transition amplitude within adiabatic theory [Eqs. (12) and (13)]. As discussed above, the standard HC approximation results from Eqs. (12) and (13) when the singularity at $v_R=0$ in Eq. (12) or, likewise, the fact that the lower limit of the integral $R(0)$ gives a significant contribution in Eq. (13), is neglected. This is also equivalent to the neglect of the preexponential factor in the quasi-classical approximation [Eq. (31)]. However, as already noted by Landau [14], the presence of additional singularities in the transition matrix element near the turning point may give rise to corrections. In this section we explicitly determine these contributions and show that they can alter the adiabatic limit in a profound way by modifying the exponential decay behavior.

The starting point is the observation that near the turning point, the adiabatic coupling matrix element $U_{f,i}[R(0)]$, in general, does not vanish. For any finite value of the coupling at the TP, $U_{f,i}[R(0)]\neq 0$, closing the contour of integration is more involved than implied by a single branch point (Fig. 1). The analysis of the integration path can be performed either in the complex t or complex R domains. Here we adopt the former (see [29] for the latter). Figure 2 illustrates a proper closing of the integration contour. The integrand in Eq. (11) has branch points and single poles at $vt_c=\pm\sqrt{R_c^2-b^2}$, $\pm\sqrt{(R_c^*)^2-b^2}$ originating from the adiabatic energy surface and nonadiabatic coupling $U_{f,i}$. In addition, the radial velocity in the integrand has branch points at

$$vt_v=\pm ib, \tag{46}$$

where b is the impact parameter. As long as $U_{fi}[R(0)]\neq 0$, there is an additional contribution to the transition defined by the integral over a loop encircling the branch point that does not originate in the adiabatic energy surface, but in the nonadiabatic matrix element that contains the radial velocity. A possible effect of the branch points of the radial velocity was recognized recently by Ostrovsky [30]. However, only the correction to the dynamical phase of the hidden crossings transition for $b=0$ was considered, missing the TP effect we described here.

The contour in Fig. 2 has been chosen to avoid the branch cuts of both v_R and $E_{i,f}$, thus keeping integration on a single-valued Riemann sheet. Using Cauchy's theorem, the integral over the whole contour is zero (i.e., no pole is enclosed). Therefore, assuming that the integral over the upper half plane is zero, the S-matrix element for the two-state system, which is equal to the integral over the real axis, becomes

$$S_{f,i}=S_{f,i}^{\mathrm{HC}}+S_{f,i}^{\mathrm{TP}}, \tag{47}$$

where $S_{i,f}^{\mathrm{HC}}$ arises from the loops avoiding the branch cuts of $U_{i,f}$. In addition to the HC contribution, the S matrix contains a TP correction term, $S_{i,f}^{\mathrm{TP}}$, given by the integral over the loop avoiding the branch cut of v_R. Since t in this loop is purely imaginary, we can define a real variable $y=vt/i$ such that the correction term to the S matrix becomes

$$S_{f,i}^{\mathrm{TP}}=-2i\,\mathrm{Re}\left\{\int_b^\infty dy\,\frac{y}{\sqrt{y^2-b^2}}\,U_{f,i}(i\sqrt{y^2-b^2})\times\exp\left[-\frac{1}{v}\int_0^y dy'\,\Delta E_{f,i}(iy')\right]\right\}. \tag{48}$$

This integral is difficult to evaluate analytically, even if a Lorentzian coupling [Eq. (40)] is assumed. Moreover, the Lorentzian is not an accurate description of the nonadiabatic matrix element far from R_C. Therefore the actual value of $U_{f,i}$ needs to be used in the evaluation of the integral in Eq. (48). We have evaluated this integral by the following expansion that provides a very accurate approximation to the exact result. Since the integrand in Eq. (48) has an integrable singularity at $y=b$ and decreases exponentially with increasing b, the largest contributions to S^{TP} must arise from $y\simeq b\simeq 0$. Thus, assuming that $\Delta E_{f,i}(R\approx 0)\simeq\Delta E(0)=\Delta$ is constant and making a change of variables $\cosh z=y/b$,

$$S_{f,i}^{\mathrm{TP}}\simeq -2ib\,\mathrm{Re}\left\{\int_0^\infty dz\,\cosh z\,U_{f,i}(ib\sinh z)\times\exp(-\lambda\cosh z)\right\}, \tag{49}$$

where $\lambda=b\Delta/v$. Expanding $U_{f,i}$ in powers of b,

$$U_{f,i}(ib\sinh z)\simeq U_{f,i}(0)+ib\sinh z\left.\frac{dU_{f,i}}{dR}\right|_0+\frac{(ib\sinh z)^2}{2}\left.\frac{d^2U_{f,i}}{dR^2}\right|_0+\cdots, \tag{50}$$

one finds [31]

$$S_{f,i}^{\mathrm{TP}}=-2ib\left[K_1(\lambda)U_{f,i}(0)+\sum_{n=1}^{\infty}(-1)^n b^n\left(\frac{v}{\Delta}\right)^n\times\frac{(2n-1)!!}{(2n)!}K_{n+1}(\lambda)\frac{d^{2n}}{dR^{2n}}U_{f,i|R=2}\right], \tag{51}$$

where K_i are modified Bessel functions of the second kind. Equation (51) provides not only an expansion in b but also an expansion in v/Δ. For $U_{f,i}(0)\neq 0$ one obtains as the leading term in the adiabatic limit

$$S_{f,i}^{\mathrm{TP}}|_{v\to 0}\to -2ibU_{f,i}(0)K_1\left(\frac{\Delta b}{v}\right). \tag{52}$$

Transitions near the turning point take place effectively only inside the adiabatic cutoff radius b defined by

$$\lambda=\frac{\Delta b}{v}\lesssim 1, \tag{53}$$

i.e., when the characteristic frequency $\omega\approx v/b$ of the perturbation is at least of the order of the energy gap Δ between the energy levels near the turning point. This adiabatic cutoff radius for TP contributions is to be distinguished from the adiabatic radius a. For small impact parameters $\lambda\ll 1$, the TP transition amplitude exhibits an effective power-law dependence on the velocity. In particular, $S_{f,i}^{\mathrm{TP}}|_{b\to 0}\to -2iU_{f,i}(0)v/\Delta$ and, thus, the transition probability is proportional to v^2 in that limit. Interestingly, Born and Fock [17] predicted that the transition probability in the adiabatic limit between two adiabatic states with noncrossing energy levels cannot be larger than of order of v^2. The exactly solvable one-dimensional (1D) model of two colliding δ-function potentials moving with constant speed ($x=vt$) yields transition probability proportional to v^2 [32]. These predictions are consistent with our findings. In turn, for large impact parameters (i.e., $\lambda\gg 1$), the TP transition amplitude decreases exponentially as $\exp(-\lambda)=\exp(-b\Delta/v)$.

Clearly, the TP amplitude provides the dominant contribution to the S matrix for small impact parameters and small collision velocities. However, when $v/\Delta\ll b\ll 2|R_c|$ the HC contribution can dominate since it is independent of b while the TP contribution decreases exponentially with b.

The total cross section due to the TP contribution (in the region where the HC contribution is negligible because of its exponential decrease) follows from Eq. (51) as [31]

$$\sigma_{f,i}^{\mathrm{TP}}=2^6\pi\left(\frac{v^2/2}{\Delta}\right)^2\left[\frac{U_{f,i}^2(0)}{3\Delta^2}+\sum_{n,n'=1}^{\infty}(-1)^{n+n'}2^{2(n+n')}\times\frac{(n+1)!(n'+1)!(2n-1)!!(2n'-1)!!}{(n+n'+3)(2n)!(2n')!}\left(\frac{v^2/2}{\Delta}\right)^{n+n'}\times\frac{(d^{2n}/dR^{2n}U_{f,i})|_{R=0}(d^{2n'}/dR^{2n'}U_{f,i})|_{R=0}}{\Delta^{2+n+n'}}\right],\quad(54)$$

which reduces in the adiabatic limit, when $U_{f,i}(0)\neq 0$, to

$$\sigma_{f,i}^{\mathrm{TP}}=2\pi\int_0^{\infty}db\,b|S_{f,i}^{\mathrm{TP}}(b)|^2\approx\frac{64}{3}\pi\left|\frac{U_{f,i}(0)}{\Delta E_{f,i}(0)}\right|^2\left(\frac{\frac{1}{2}v^2}{\Delta E_{f,i}(0)}\right)^2.\quad(55)$$

Remarkably, this contribution increases with the fourth power of v, or equivalently, with the square of the equivalent kinetic energy of the electron in units of the energy gap at $R=0$. Its size is controlled by the ratio of the nonadiabatic coupling to the energy splitting at $R=0$. As $v\to 0$, this term, unlike the exponentially suppressed HC contribution, gives the dominant adiabatic limit for the inelastic cross section. If $U_{f,i}=0$, as is the case for symmetric ion-atom collision systems (e.g., $H^+ + H$), the TP contribution to the cross section is given by the higher orders in the expansion in the impact parameter and the cross section is proportional to v^8 and to the square of $d^2U_{f,i}(0)/dR^2|_0$. Explicitly,

$$\sigma_{f,i}^{\mathrm{TP}}\approx\frac{9}{5}\times 2^{10}\pi\left|\frac{d^2U_{f,i}(R)/dR^2}{[\Delta E_{f,i}(R)]^2}\right|_{R=0}^2\left(\frac{\frac{1}{2}v^2}{\Delta E_{f,i}(0)}\right)^4.\quad(56)$$

Note that Eqs. (51)–(56) are valid irrespective of the particular form of the adiabatic coupling matrix element $U_{f,i}(R)$ or the shape of the potential curves $E_{f,i}(R)$. Furthermore, the expressions for the TP transition probability and the cross section are independent of the existence of a branch point between the adiabatic energies. Therefore, S^{TP} not only provides a correction to the adiabatic behavior predicted by the HC theory but also yields nonzero transition probabilities for pairs of adiabatic levels that are not connected by branch points and, therefore, vanish within the LZ or HC approximations. In principle, the TP and HC contributions to the transition amplitude could overlap. However, since the width ΔR of HC and LZ transitions become very small as $v\to 0$ [see Eq. (41)], the overlap can be, in most cases, safely neglected.

Up to this point we have only considered TP contributions to the S matrix for a two-level system. It may be useful to extend the description of the TP transitions to multilevel HC approximations. The underlying idea is that the TP transition is approximately localized near the turning point. Therefore, one can simply add one more local time-evolution matrix around $t=0$ [see Eq. (45)]. The additional local time evolution can be constructed by adding all the two-state TP S-matrix elements among all states coupled. Within the CCHC method described in the previous section, the TP-like contribution, even though not necessarily correct, is implicitly included in the numerical evaluation of the MOCC equations [Eq. (6)] since for Lorentzian coupling elements we have in general $U_{f,i}^{\mathrm{LZ}}[R(0)]\neq 0$. Since $U_{f,i}^{\mathrm{LZ}}[R(0)]$ will differ from the exact $U_{f,i}[R(0)]$, TP corrections must be explicitly built into the CCHC calculation. If we want to recover the pure $S_{f,i}^{\mathrm{HC}}$ matrix excluding TP contributions from the numerical CCHC scheme, we have to subtract the incorrect TP contribution

$$S_{f,i}^{\mathrm{HC}}\simeq S_{f,i}^{\mathrm{CCHC}}+2ibU_{f,i}^{\mathrm{HC}}(0)K_1\left(\frac{\Delta E_{f,i}(0)}{v}b\right).\quad(57)$$

The error of the CHCC method is given by the difference between the true $U_{f,i}$ near the turning point and the coupling matrix element $U_{f,i}^{\mathrm{HC}}$ extrapolated to the turning point. Consequently, the approximate S matrix corrected for turning point effects is therefore given by

$$S_{f,i}^{\mathrm{HC+TP}}\simeq S_{f,i}^{\mathrm{CCHC}}+2ib[U_{f,i}^{\mathrm{HC}}(0)-U_{f,i}(0)]K_1\left(\frac{\Delta E_{f,i}(0)}{v}b\right).\quad(58)$$

Alternatively, one can improve the CCHC method by correcting the coupling matrix element used in the numerical integration of Eq. (6) as

$$U_{f,i}^{\mathrm{HC+TP}}(R)\simeq U_{f,i}^{\mathrm{HC}}(R,R_c)+[U_{f,i}(0)-U_{f,i}^{\mathrm{HC}}(0)]\times\exp\left(-\frac{\Delta E_{f,i}(0)}{v}R\right).\quad(59)$$

This approximate form incorporates this correction within the ''radius of nonadiabaticity'' of the TP.

IV. NUMERICAL TESTS FOR AN EXACTLY SOLVABLE MODEL

In this section we present results of the first detailed numerical test for the validity of the HC approximations and its variants as well as for the significance of TP contributions. We perform this test for a simple 1D model of a symmetric collision in which the target and the projectile are represented by harmonic wells,

$$H_{\mathrm{el}}(R)=\frac{p^2}{2}+\frac{1}{2}\left(|x|-\frac{R}{2}\right)^2,\quad(60)$$

where x and p are the position and momentum of the electron with respect to the center of mass of the collision system. In order to mimic the radial velocity in a 3D collision, we use the parametric dependence $R=\sqrt{v^2t^2+b^2}$, which corresponds to a 3D straight-line internuclear motion for a given impact parameter b.

The advantage of studying this simple collision system is that exact transition probabilities can be easily obtained by numerically solving the time-dependent Schrödinger equation (TDSE)

$$i\frac{\partial}{\partial t}\Psi_{v,b}(x,t)=H_{\mathrm{el}}\Psi_{v,b}(x,t),\quad(61)$$

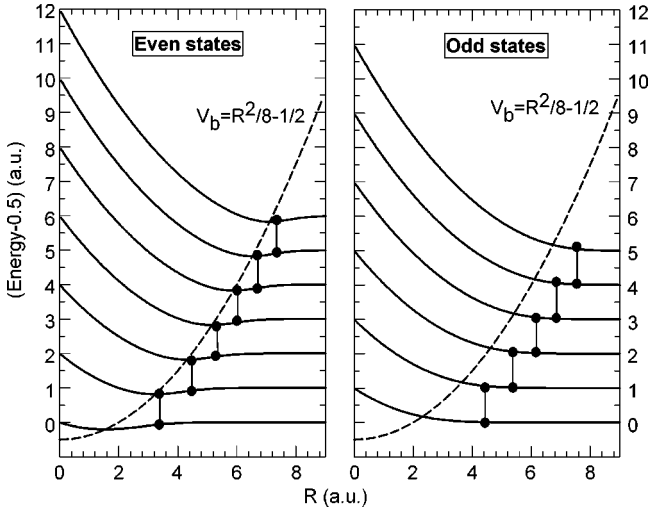

FIG. 3. Adiabatic energy terms for the double harmonic oscillator (solid lines). The energies are shifted down in 0.5 a.u. so that the terms E_N tend to N for $R\rightarrow 0$. The top of the potential barrier, $V_s(R)$ (dashed line) is compared with the positions of the hidden crossings connecting adjacent energy terms (solid circles connected with vertical lines).

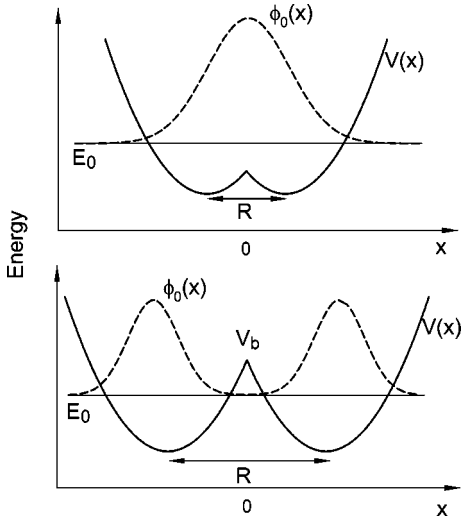

FIG. 4. Schematic diagram of the total electronic potential (solid line), and the ground-state energy E_0 (horizontal solid lines), and wave function ϕ_0 (dashed line) for two internuclear distances. The top of the potential barrier, V_b, is also depicted.

where $\Psi_{v,b}$ is the electronic wavefunction for a given impact parameter and a given collision velocity. Moreover, this system can serve as a model system to illustrate the significance and the physical origin of hidden crossings since this system features only HCs of the Q-type [3] while narrow avoided crossings are absent. The obvious drawback of this model is that no conclusions as to the quantitative significance of the scattering amplitudes and, specifically, of turning point effects can be drawn. As this model strongly differs from the atomic Coulomb systems, the importance of a particular process at a given velocity cannot be determined. This should be kept in mind as we present numerical results in atomic units.

A. Hidden crossings in the adiabatic eigenenergy curves

The ''molecular'' adiabatic eigenstates, $|\phi_N(R)\rangle$ and eigenenergies, $E_N(R)$ of $H_{\rm el}(R)$ [Eq. (60)] are well known and can be found in quantum mechanics text books (see, e.g., [33]). The presence of hidden crossings in the system appears to have been overlooked. These energy levels are depicted in Fig. 3. In the limit $R\rightarrow 0$, the system becomes a single harmonic oscillator with $E_N\rightarrow(N+0.5)$. In turn, for $R\rightarrow\infty$ the system develops into two well-separated harmonic wells with $E_N\rightarrow([N/2]+0.5)$, where [ ] denotes the integer part. The only exact symmetry for the adiabatic wave functions is the reflection symmetry with respect to the origin of coordinates $(x=0)$. This yields two sets of mutually noninteracting adiabatic molecular states defined with even and odd integers N, for the symmetric and antisymmetric wave functions, respectively.

The energy levels in Fig. 3 do not exhibit any obvious avoided crossing. However, the present system is rich in hidden crossings denoted by vertical lines between adiabatic curves connected by branch points. On the real axis, hidden crossings can be characterized by the fact that for the minimal distance between energy curves at the hidden crossings, $\Delta E(R_{\rm HC})$, is of the same order as the average energy level spacing $\overline{\Delta E}$ of nearest neighbors,

$$\Delta E(R_{\rm HC})\lesssim\overline{\Delta E}. \tag{62}$$

This is to be contrasted with narrow avoided crossings where

$$\Delta E(R_{\rm AC})\ll\overline{\Delta E}. \tag{63}$$

The physical origin of hidden crossings is obviously closely connected to the existence of a barrier separating the two wells, as indicated by the close correlation between the R-dependence of the barrier top, $V_b=R^2/8$ and the position of the series of HC's (Fig. 3). Unlike Coulomb systems [34], the barrier top in the present case does not form a saddle but a cusp (Fig. 4). The existence of HC in the present case illustrates that the detailed analytic form of the barrier, in particular the presence of saddles, is irrelevant for the formation of HC's. The hidden crossings emerge when the top of the moving barrier crosses the quasimolecular term. For example, at the beginning of the receding phase of a collision [Fig. 4(a)] the target and the projectile are close and an electron wave function is shared between the two centers, being molecular in character. A single classically allowed region for the electronic motion extends over both wells. While the centers are receding, the rising potential barrier crosses the molecular energy level and splits the classically allowed region into two separate domains [Fig. 4(b)]. Semiclassically, the addition of two turning points leads to a jump of the Maslov index by $\pi/2$. Accordingly, the quantum wave function undergoes a rapid morphological change [Fig. 4(b)] which, in turn, causes a peak in the matrix element of the d/dR operator, as can be directly seen in Fig. 5.

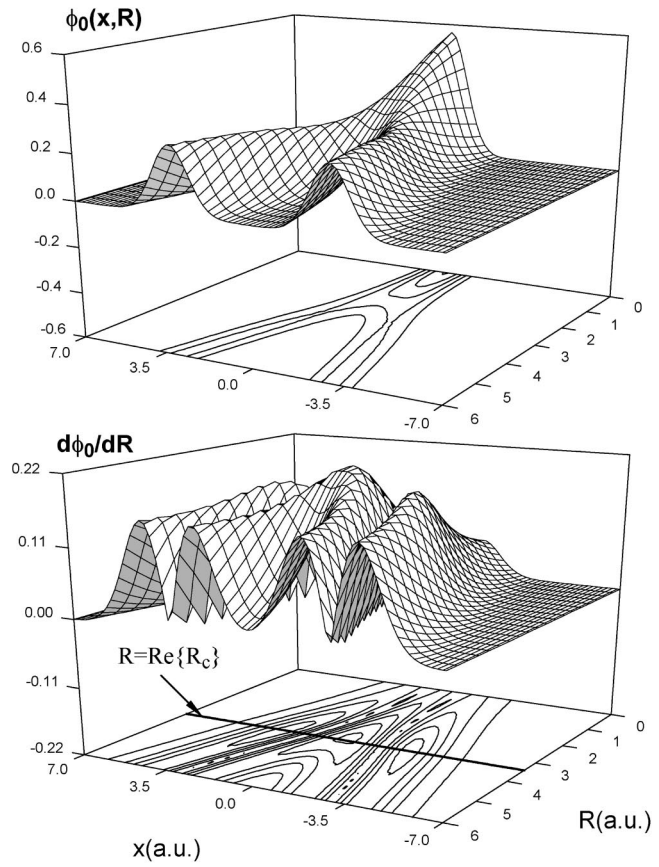

FIG. 5. Ground quasimolecular state and its derivative as a function of the electronic coordinate x and the internuclear distance R.

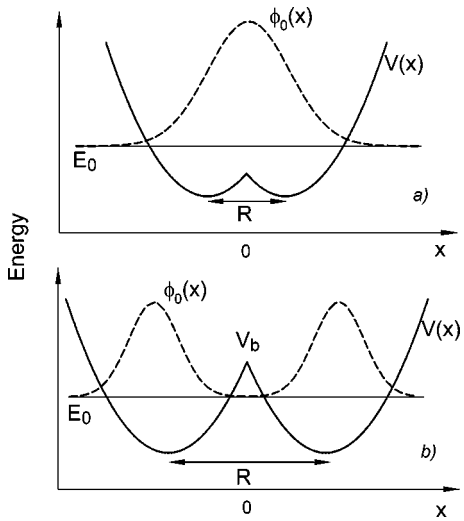

FIG. 6. The positions of branch points in the plane of complex internuclear distance R (hollow symbols) and their corresponding scaled Massey parameters, $\delta_{f,i}=v\,\mathrm{Im}\{\omega_c\}$ (solid symbols). The numbers i-j $(i,j=0,1,2,3,...)$ in the figure denote the energy levels that become connected by the branch points. Hidden crossings that connect the same Riemann energy surfaces correspond to different orders (0,1,2,...) and are connected by lines starting from the zeroth-order (i.e., the ones with the smallest imaginary parts).

Figure 4(b) can also serve as an illustration for the mechanism underlying the presence (or absence) of avoided crossings. The generic picture of the occurrence of an avoided crossing is that of a weak residual interaction between two nearly degenerate levels. The near degenerate ($H_{11}\simeq H_{22}$) levels can be pictured as the two ''split'' levels in the right and the left wells after they lie below the barrier top in Fig. 4(b). Accordingly, the residual interaction (i.e., the diabatic coupling H_{12}) represents the tunneling through the barrier and is therefore exponentially weak which, in turn, immediately explains the relation (63). In general, Fig. 4(b) would correspond to a cut of a multidimensional potential surface along a ''reaction coordinate.'' In the present 1D case, however, parity in the x coordinate is an exact symmetry. Therefore, the (un)gerade linear combinations of the ''partial'' wave functions residing in the different wells belong to different representations of the symmetry group and therefore the coupling H_{12} vanishes identically. By contrast, hidden crossing refers to coupling between neighboring nondegenerate (as opposed to near degenerate) levels of the same symmetry where one level has just crossed the barrier and the wave function is about to split while its nearest neighbor lies still above V_b. This observation results immediately in the relation (62). Figures 4 and 5 also illustrate why HC's appear in series. The origin is twofold: for one, as level E_n crosses the barrier from above and causes the wave function to ''split'' all other wave functions of the same symmetry must also undergo a change because of the orthogonality constraints for all ϕ_m $(m\neq n)$ at a fixed value of R_{HC}. This can lead to couplings not only between adjacent levels n and $n+1$ but to all other levels as well. In Coulomb systems, this is called a Q series [2,6–8]. Its signature are branch points occurring at the same $R_{\mathrm{HC}}=\mathrm{Re}\{R_C\}$ but rapidly increasing $\mathrm{Im}\{R_C\}$ corresponding to weaker couplings to distant levels. In the present case, presumably because of the constancy of the mean spacing in oscillator systems, only the nearest neighbor coupling can be observed (Fig. 6). A second mechanism for the generation of series is the fact that with increasing R subsequently higher adiabatic levels cross the barrier from the top. This sequence of branch points with varying $R_{\mathrm{HC}}(n)$ is called the ''superseries'' in Coulomb systems [6–8]. Obviously, it appears in the present case as well (Fig. 6). While we have only found branch points connecting adjacent energy levels, they appear in different orders (increasing values of $\mathrm{Im}\{R_c\}$ and $\mathrm{Re}\{R_c\}$), much like for the so-called P series [2] which, in the Coulomb case, describe the nonadiabatic coupling of the Demkov-type between two parallel almost degenerate diabatic levels. However, a P series in the Coulomb case is located at an almost constant value of $\mathrm{Re}\{R_c\}$, which is not the case here. This is, in part, a consequence of large energy splitting between the levels. In order to visualize the different orders of transitions between the same pair of energy levels, we have connected the corresponding branch points for different orders by lines. Interestingly, these lines are almost parallel to the $\mathrm{Im}\{R_c\}=\mathrm{Re}\{R_c\}$ line that corresponds to an angle in the complex plane of $\theta=\pi/4$ [i.e., $R=|R|\exp(i\theta)$]. In addition, the hidden crossings of the same order but connecting different pairs of

states [35] have all similar values of the imaginary part, $\mathrm{Im}\{R_c\}$. No branch points were found with a phase angle larger than $\pi/4$. Also plotted in the figure are the values of the scaled Massey parameter $\delta_{f,i}=v\ \mathrm{Im}\{\omega_c\}$, which is independent of velocity. Since the Massey parameter $\mathrm{Im}\{\omega_c\}$ [Eq. (29)] is approximately proportional to $\mathrm{Im}\{R_c\}$ and the energy splitting at $\mathrm{Re}\{R_c\}$ are here approximately unity, the values of $\delta_{f,i}$ as a function of $\mathrm{Re}\{R_c\}$ lie very close to the branch points. Since transition probabilities decrease exponentially with $\delta_{f,i}$, the relative contribution of each order decreases very rapidly with increasing order of the transition.

The important role played by the top of the barrier explains also the large difference between the Massey parameters for even and odd adiabatic energy eigenstates (Fig. 6). The Massey parameters for odd states are about 1 a.u. larger than the ones for even states. This is due to the fact that the odd wave functions have a node at the position of the top of the barrier, $x=x_b=0$. Therefore, the rate of change of the wave function with R diminishes as the level falls below the barrier top.

Even though hidden crossings are difficult to visually detect as avoided crossings for real values of R, they become evident in the complex R plane where energy levels cross at the branch points. This is shown in Fig. 7(a) where we depict the real parts of the energies of the $N=0$ and $N=2$ adiabatic states. The energy levels in this figure are displayed as a function of $\mathrm{Re}\{R\}$ along a ray $R=R\exp(i\theta)$, where $\theta=23°$ is a constant. This particular angle has been chosen such that the ray passes very close to the zero-order hidden crossing between the $N=0$ and $N=2$ levels, which occurs at $R_c=(3.41,1.62)$ and $\theta\simeq 25°$. Obviously, the energy levels exhibit an avoided crossing in the neighborhood of the branch point. The branch point is responsible for the singular behavior of the adiabatic coupling between the $N=0$ and $N=2$ states [i.e., Eq. (40)]. Figures 7(b) and 7(c) show that other variables of the system such as the derivative of the complex eigenergy, dE_0/dR, and the norm of the wave function $|c_0|$ (see Sec. III) also become singular at the branch point.

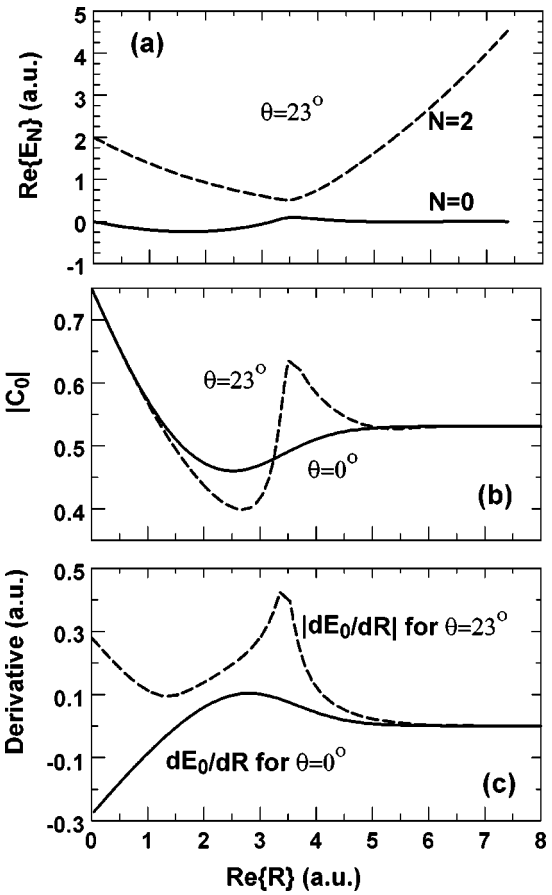

FIG. 7. (a) $\mathrm{Re}\{E_0\}$ and $\mathrm{Re}\{E_2\}$ as a function of $\mathrm{Re}\{R\}$ along a ray in the complex R plane with an angle of $\theta=23°$. (b) and (c) the derivative of E_0 with respect to R and the normalization constant of the $N=0$ adiabatic state along two rays in the complex R plane are compared ($\theta=0°,23°$). The branch point between the $N=0$ and $N=2$ states lies on the ray of approximately $\theta=25°$ at $\mathrm{Re}\{R_c\}=3.41$ a.u.

B. Transition probabilities and cross sections

In this subsection we analyze the transition probabilities and cross sections for the model Hamiltonian in Eq. (60). We study the time evolution of this system for the case in which initially (at $t\to-\infty$) the $N=0$ state is populated. This limits the allowed transitions to excitation of the subset of even adiabatic states.

Figure 8 displays the excitation probabilities to the $N=2$ level for $b=0.1$ a.u. as a function of the inverse velocity $1/v$. In this representation an exponential decrease of the probability, $\exp(-\mathrm{const}/v)$, reduces to a straight line, as is clearly observed for the HC excitation probability, averaged over all phases (HCE). Remarkably, the low-velocity behavior (large $1/v$) of the TDSE excitation probability is quite different from an exponential dependence. This is a direct consequence of the TP contribution to the transition probability [Eq. (48)]. Also included are the results of the CCHC method involving seven excited states ($N=0,2,6,8,10,12,14$), taking into account the first-order (CCHC1) and, the first- and second-order (CCHC2) hidden crossings between a same pair of states. Unlike the single-path HC approximation, the presence of different paths within the CCHC allows for interference oscillations (the so-called Stückelberg oscillations). Furthermore, the CCHC calculations also predict a large deviation from the exponential decay of the transition probability as resulting from the inclusion of TP effects since

$$U_{f,i}^{\mathrm{HC}}(0)=\frac{\mathrm{Im}\,R_c}{2|R_c|^2}\neq 0. \tag{64}$$

This TP effect is here spurious since $U_{f,i}^{\mathrm{HC}}(0)$ obtained from Eq. (40) is not expected to have a correct value at $R=0$. The coupling described by Eq. (40) is designed to be accurate in the vicinity of hidden crossings only. As can be seen from the figure, both CCHC1 and CCHC2 give, as expected, the same result in the ''hidden crossings region'' i.e., in the region where transitions due to the hidden crossings dominate, but very different results for larger values of $1/v$, where the TP effect dominates. This difference emerges from

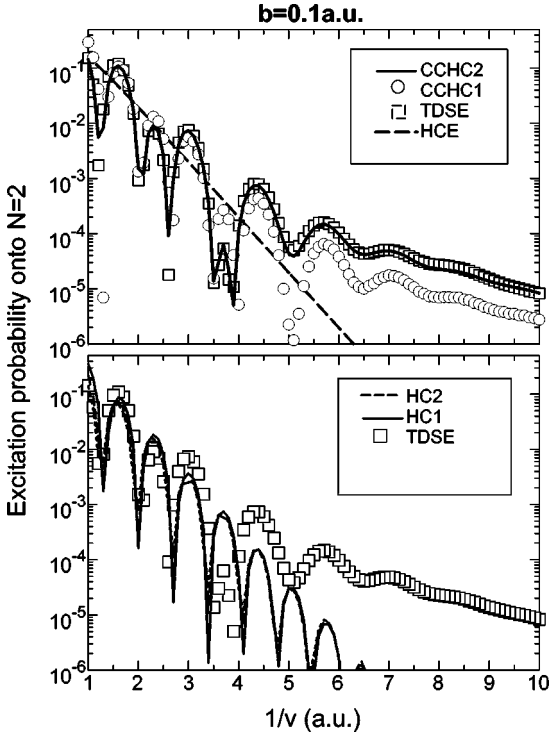

FIG. 8. Excitation probability onto the $N=2$ level for $b=0.1$ a.u. as a function of the inverse velocity $1/v$. The TDSE results are compared with the HCE and HC results and, with CCHCn calculations involving up to n orders of hidden crossings.

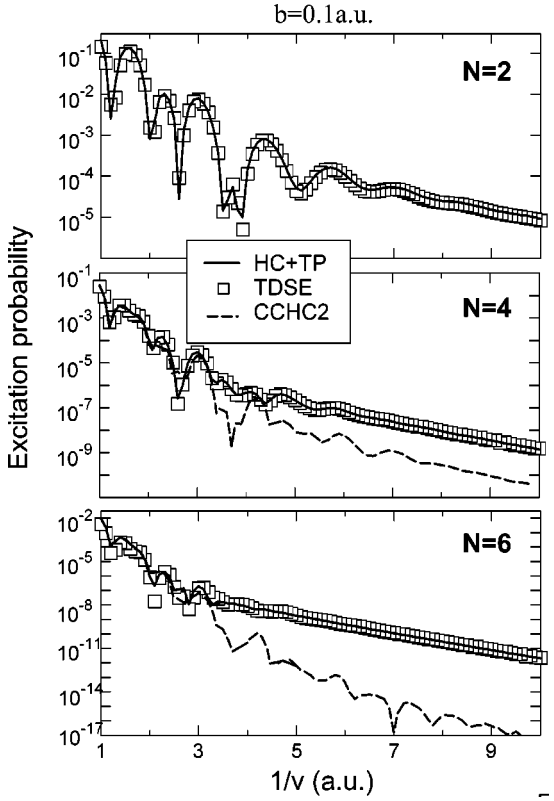

FIG. 9. Excitation probability onto the $N=2$, 4, 6 levels for $b=0.1$ a.u. as a function of the inverse velocity $1/v$.

the difference between $U_{f,i}^{\mathrm{HC1}}(0)$ and $U_{f,i}^{\mathrm{HC1}}(0)+U_{f,i}^{\mathrm{HC2}}(0)$ in the CCHC1 and CCHC2 calculations. Incidentally, $U_{f,i}^{\mathrm{HC1}}(0)+U_{f,i}^{\mathrm{HC2}}(0)$ between the levels $N=0$ and 2 has almost the same value as the exact coupling $U_{f,i}(0)$, thus leading to very good agreement of the CCHC2 and TDSE results even at the lowest v. Subtracting these spurious contributions according to Eq. (57) yields (referred to in the following as HC), as expected, an exponentially decaying excitation probability superimposed on well-known Stückelberg oscillations (HC1 and HC2 in Fig. 8). If we now add to these HC amplitudes the correct TP contribution according to Eq. (58) we refer to these calculations as HC+TP.

Figure 9 displays the excitation probabilities to the $N=2$, 4, and 6 levels for $b=0.1$ a.u. as a function of the inverse velocity $1/v$. Remarkably, the HC+TP calculations are found to be in very good agreement with the TDSE results for all N, as well as with the CCHC2 calculations for excitation to $N=2$. It is noteworthy that the TP contribution for excitation onto $N=4$ and $N=6$ states involves the direct couplings from the $N=0$ level, $U_{4,0}(0)$ and $U_{6,0}(0)$. These direct couplings are not contained in the standard HC approximation because the $N=0$ level is not connected to the $N=4$ and 6 levels by branch points. The CCHC2 calculation also yields excitation to $N=4$ and 6. This is due to the sequential HC couplings and, due to spurious $0\rightarrow 2$ and $2\rightarrow 4$ TP contributions for larger $1/v$ in the CCHC calculations, which are here not eliminated by the subtraction procedure [Eq. (57)]. Note, however, that this is a second order process and, therefore, the excitation probability by consecutive transitions is much smaller than the direct $0\rightarrow 4$ transition.

The dependence of the transition probabilities on the impact parameter, for a fixed velocity of $v=0.2$, is shown in Fig. 10. The TDSE result for excitation to both $N=2$ and $N=4$ is again well reproduced by the HC+TP calculations. For comparison, also the HC calculation, that is, the CCHC solution with the spurious TP contribution subtracted, is shown. Obviously, at large impact parameters outside the adiabatic cutoff for turning-point contributions [Eq. (53)], the HC approximation works well. Figure 11, which displays the excitation probability as a function $1/v$ for a ''large'' impact parameter $b=1$ a.u., shows that this conclusion is valid at all collision velocities. By contrast, inside the adiabatic radius the TP contributions dominate and the HC approximation breaks down (see Figs. 9 and 10). For excitation to $N=4$ the TDSE results are also well reproduced by the TP+HC calculations since the TP contribution from the direct coupling between the $N=0$ and $N=4$ levels is included.

The relative importance of different excitation processes averaged over impact parameters as a function of collision velocity can be extracted from the excitation cross sections (Fig. 12). The total cross sections for excitation to $N=2$ and 4 calculated with the HC+TP approach is seen to agree extremely well with the results of the TDSE calculations. The crucial point to be noted is that the standard HC approximation predicts cross sections at larger (though limited from above by $v\lesssim 1$) velocities accurately but leads to large discrepancies for small v due to its exponential decay with $1/v$

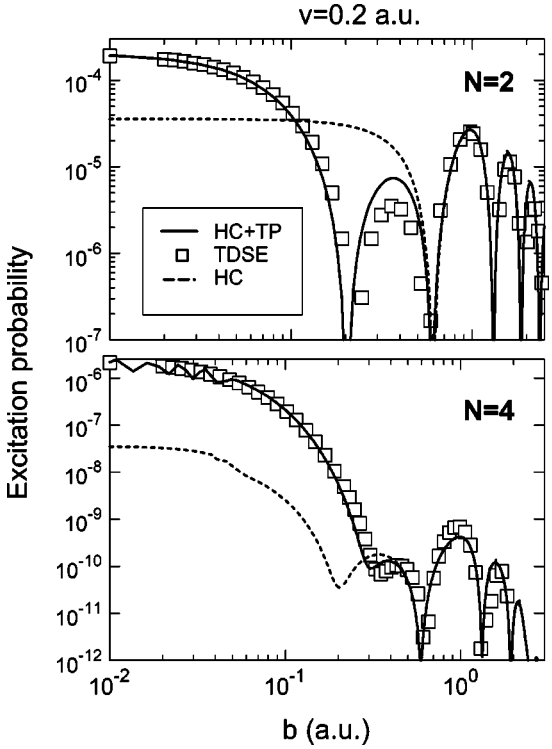

FIG. 10. Excitation probability onto the $N=2$, 4 levels for $v=0.2$ a.u. as a function of the impact parameter.

while the correct adiabatic limit features a power law ($\approx v^4$) arising from the TP contribution. The transition region in which the TP contribution starts to dominate the cross section is located at larger velocities for excitation to $N=4$ ($v\approx 0.24$) than for excitation to $N=2$ ($v\approx 0.16$). The Stückelberg oscillations observed in the previous figures for a fixed velocity or a fixed impact parameter are averaged out in the cross section.

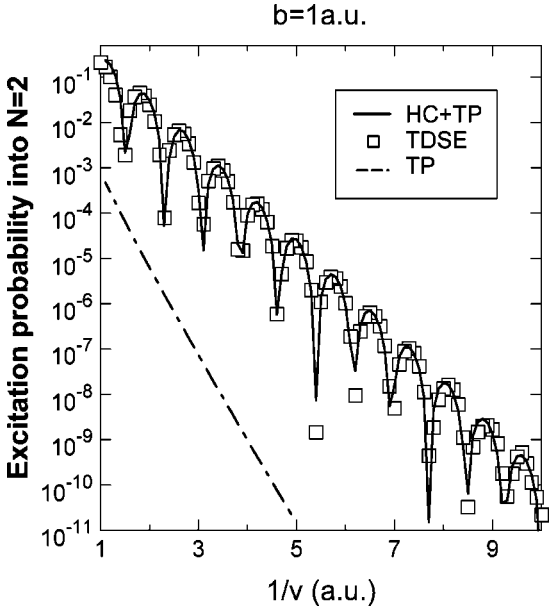

FIG. 11. Excitation probability onto the $N=2$ level for $b=1$ a.u. as a function of the inverse velocity $1/v$.

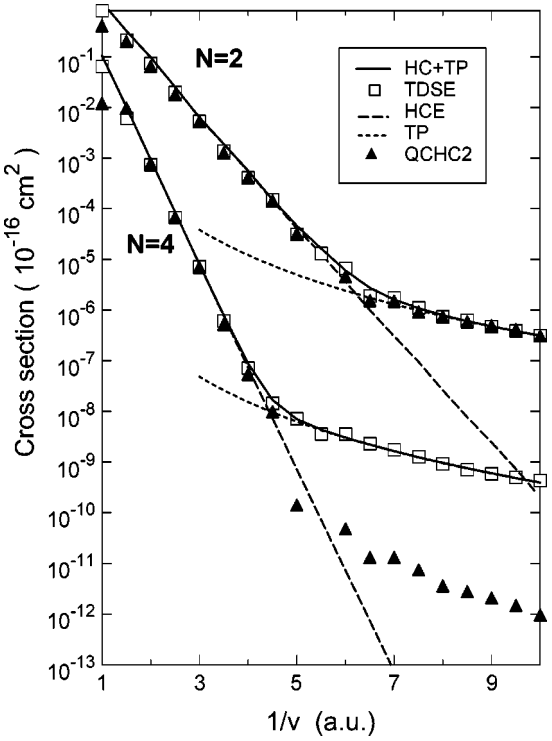

FIG. 12. The cross sections for excitation from $N=0$ onto $N=2$ and $N=4$ as a function of the inverse velocity.

In order to ascertain the significance of TP effects, we have performed two additional checks: one test concerns the breakdown of the classical-trajectory approximation underlying our analysis. Since turning-point effects could potentially be contaminated by the breakdown of the classical trajectory description underlying the impact-parameter method, we have also embedded the 1D model Hamiltonian Eq. (60) into a 3D model, in which the internuclear motion is described quantum mechanically by solving for each angular momentum, ℓ, the radial Schrödinger equation [36,37]

$$\left(-\frac{1}{2\mu}\frac{\partial^2}{\partial R^2}+\frac{\ell(\ell+1)}{2R^2}+H_{\rm el}(R,x)\right)\Psi_\ell(x,R) = E_T\Psi_\ell(x,R), \tag{65}$$

where μ is the reduced internuclear mass, E_T is the total energy, and $\Psi_\ell(x,R)$ is the total wave function for a given angular momentum ℓ of nuclear motion. This quantum coupling (QC) problem can be solved exactly as well. Artifacts due to the classical description of the trajectory near the turning point are therefore ruled out. We use a typical value of $\mu=1$ amu, seven adiabatic states to expand the electronic wave function, and, in order to simplify the calculations, we solve Eq. (65) using the approximate HC coupling matrix elements [Eq. (40)] and a log-derivative algorithm [37]. Such QCHC calculations (referred to as QCHC2 in Fig. 12) agree extremely well with the classical trajectory cross sections (TDSE and HC+TP) for excitation to $N=2$, while strongly deviate from the TDSE result for excitation to $N=4$. This is for the reasons discussed below Eq. (64), since QCHC2 does not have the correct coupling at the TP (like in Figs. 8 and

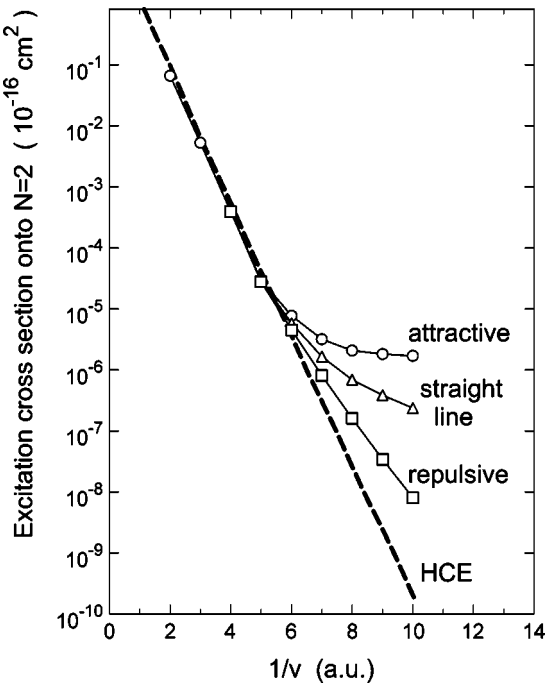

FIG. 13. The cross sections for excitation from $N=0$ onto $N=2$ as a function of the inverse velocity. The HC result is compared with QC calculations involving different internuclear interactions: attractive $V_{\mathrm{nuc}}(R)=-\exp(-2R)/R$, repulsive $V_{\mathrm{nuc}}(R)=\exp(-2R)/R$, and no interaction (straight line).

9). The velocity region where the TP effect starts to dominate the cross section is near $v\sim 0.2$, which would correspond to a collision energy of 1 keV/amu. Clearly, this energy is high enough to apply the classical straight-line trajectory approximation for the internuclear motion. The HC theory is applicable above this energy up to $v\simeq 1$, which corresponds to a collision energy of 25 keV/amu.

A second test considers trajectory effects. Transitions near the TP in realistic collisions can be influenced by the interaction potential between the heavy nuclei. Therefore, we have investigated the effect of the internuclear interaction on the transition probabilities within the QCHC approach by incorporating a potential $V_{\mathrm{nuc}}(R)=\pm\exp(-2R)/R$, where the sign of the potential determines whether the interaction is attractive or repulsive. Figure 13 compares the results of such calculations with the one obtained for a ''straight-line trajectory'' [i.e., $V_{\mathrm{nuc}}(R)=0$]. For ''high'' velocities, the internuclear interaction does not affect the value of the cross sections. However, cross sections become quite sensitive to the particular form of this interaction in the limit of low velocities. As is intuitively expected, an attractive (repulsive) potential increases (decreases) the value of the cross section. The increase (decrease) can be ascribed to the different topologies of the radial velocity in these cases and the fact that at the TP of the trajectory for an attractive (repulsive) interaction the nuclei get closer (farther) to each other. The point to be noted, however, is that both calculations for an attractive or a repulsive potential differ from the HC predictions and the differences are, once again, due to the TP contribution.

V. CONCLUSIONS

We have analyzed the physical contents and the limits of validity of the hidden crossings and quassiclassical approximations in near-adiabatic inelastic collisions. We have shown that the HC approximation follows from the adiabatic perturbation theory as a special case when only singularities associated with branch points of the adiabatic energy surfaces are taken into account. Since the transition matrix element in adiabatic perturbation theory contains, in general, other singularities, specifically those connected to turning points, corrections arise that are neglected in the HC approximation. We have shown that TP corrections can fundamentally alter the adiabatic limit giving rise to a power law dependence v^n rather than an exponential dependence as a function of the inverse velocity v^{-1}. This result holds irrespective of the detailed properties of the systems under consideration or of the details of description of internuclear motion.

For an accurate description of the TP effect only two parameters are needed: the energy splitting and the radial coupling of the adiabatic states near the united atom limit. The dominance of the TP effect requires: $U_{i,j}(0)\neq 0$ and $\Delta E_{i,j}(0)\neq 0$. When $\Delta E_{i,j}(0)=0$, transitions for small R can result in nonexponential behaviors of the cross section but for different reasons. A prominent example of this kind is the transition between the rotationally coupled states, which is beyond the scope of this paper.

We have illustrated properties of hidden-crossing approximations and turning-point contributions with the help of a simple, exactly solvable model. It should be noted, however, that the results can serve only as qualitative illustration of the underlying effects and not as evidence for their quantitative significance for atomic collision systems at a given set of parameters (e.g., velocity) since the present system is very different. Nevertheless, the results of the present work have implications for the application of hidden crossings or Landau-Zener approximations to atomic collisions and other time-dependent problems. ''Turning-point effects'' are, in fact, generic. Examples include the ramping up and down of an external field from $F(-\infty)=0$ to $F_{\max}=F(0)$ and back to $F(\infty)=0$ featuring an effective turning point at $F(0)$, where the slope dF/dt changes sign, since levels mixed by the field, in general, are not decoupled at $F(0)$, i.e., $U_{i,f}(0)\neq 0$. Likewise, photodissociation, starting at an equilibrium distance of the molecular constituents and approaching infinity, may feature TP corrections due to the vanishing radial velocity ($v_R=0$) at the initial condition for dissociation.

ACKNOWLEDGMENTS

P.S.K. and C.O.R. acknowledge support from the U.S. DOE, OFES, and OBES through ORNL, managed by UT-Battelle, LLC under Contract No. DE-AC05-00OR22725. J.B. acknowledges support from the FWF (Austria).

[1] E. A. Solov'ev, Zh. Eksp. Teor. Fiz. **81**, 1681 (1981) [Sov. Phys. JETP **54**, 893 (1981)].
[2] E. A. Solov'ev, Usp. Fiz. Nauk **157**, 438 (1989) [Sov. Phys. Usp. **32**, 228 (1989)], and references therein.
[3] T. P. Grozdanov and E. A. Solov'ev, Phys. Rev. A **44**, 5605 (1990).
[4] M. Pieksma *et al.*, Phys. Rev. Lett. **73**, 46 (1994).
[5] S. Y. Ovchinnikov, Phys. Rev. A **42**, 3865 (1990).
[6] R. K. Janev and P. S. Krstić, Phys. Rev. A **46**, 5554 (1992).
[7] P. S. Krstić and R. K. Janev, Phys. Rev. A **47**, 3894 (1993).
[8] P. S. Krstić, D. R. Schultz, and R. K. Janev, J. Phys. B **29**, 1941 (1996).
[9] P. S. Krstić, G. Bent, and D. R. Schultz, Phys. Rev. Lett. **77**, 2428 (1996).
[10] R. K. Janev, J. Pop-Jordanov, and E. A. Solov'ev, J. Phys. B **30**, L353 (1998).
[11] P. S. Krstić, C. O. Reinhold, and D. R. Schultz, J. Phys. B **31**, L155 (1998).
[12] L. D. Landau, Phys. Z. Sowjetunion **2**, 46 (1932).
[13] C. Zener, Proc. R. Soc. London, Ser. A **137**, 696 (1932).
[14] L. D. Landau and E. M. Lifshitz, *Quantum Mechanics (Non-Relativistic Theory)* (Pergamon, New York, 1965).
[15] E. Stückelberg, Helv. Phys. Acta **5**, 361 (1932).
[16] See, e.g., B. H. Brandsen and M. R. C. McDowell, *Charge Exchange and the Theory of Ion-Atom Collisions* (Clarendon, Oxford, 1992).
[17] M. Born and V. Fock, Z. Phys. **51**, 165 (1928).
[18] A. Messiah, *Quantum Mechanics* (Wiley, New York, 1976).
[19] E. E. Nikitin and S. Ya. Umanskii, *Theory of Slow Atomic Collisions* (Springer, Berlin, 1984), Vol. 30, Chap. 8, and references therein.
[20] A. Zwaan, Arch. Nederland IIIA **12**, 1 (1929).
[21] H. Gabriel and K. Taulberg, Phys. Rev. A **10**, 741 (1974).
[22] M. S. Child, *Semiclassical Mechanics with Molecular Applications* (Clarendon, Oxford, 1991).
[23] P. O. Lowdin, P. Froelich, and M. Mishra, Int. J. Quantum Chem. **36**, 93 (1989).
[24] K. Morokuma and T. F. George, J. Chem. Phys. **59**, 1959 (1973).
[25] V. Bykhovskii, E. E. Nikitin, and M. Ya. Ovchinnikova, Zh. Eskp. Teor. Fiz. **47**, 750 (1964) [Sov. Phys. JETP **20**, 500 (1965)].
[26] J. B. Delos and W. R. Thorson, Phys. Rev. A **6**, 728 (1972).
[27] E. E. Nikitin, *Theory of Elementary Atomic and Molecular Processes in Gases* (Clarendon, Oxford, 1974).
[28] D. S. F. Crothers, J. Phys. B **8**, L443 (1975).
[29] P. S. Krstić, C. O. Reinhold, and J. Burgdorfer, Phys. Rev. A **63**, 032103 (2001).
[30] V. N. Ostrovsky, Phys. Rev. A **61**, 032505 (2000).
[31] I. S. Gradshteyn and I. M. Ryzhik, *Table of Integrals, Series, and Products* (Academic, New York, 1980).
[32] M. Pieksma, S. Yu. Ovchinnikov, and J. H. Macek, J. Phys. B **31**, 1267 (1998).
[33] E. Merzbacher, *Quantum Mechanics* (Wiley, New York, 1970).
[34] J. M. Rost and J. Briggs, J. Phys. B **24**, 4293 (1990).
[35] R. K. Janev and P. S. Krstić, Phys. Rev. A **44**, R1435 (1991).
[36] T. G. Heil, S. Butler, and A. Dalgarno, Phys. Rev. A **23**, 1100 (1981).
[37] B. R. Johnson, J. Comput. Phys. **13**, 445 (1973).